Nonlinear Model Predictive Control for Trajectory Tracking and Obstacle Avoidance of Free-Floating Satellite Manipulator

Ali Alouache *
Centre des Techniques Spatiales, Algerian Space Agency, Arzew, Algeria.

*Corresponding Author: aalouache@outlook.com
(Received: 15-February-2024; accepted: 22-May-2024; published: 30-June-2024)
http://dx.doi.org/10.55579/jaec.202482.455

Abstract. *This paper investigates trajectory tracking with obstacle avoidance of a Free-Floating Satellite Manipulator (FFSM) under the communication failure problem. The end effector of the manipulator is desired to follow the reference path of a virtual leader while avoiding dynamic obstacles in real-time. The main idea behind this work is the use of a nonlinear model predictive controller (NMPC) with a robust optimization approach to achieve the path following and real-time collision avoidance with predefined objectives subject to the input, output and obstacle constraints. While on-line quadratic programming is adopted to achieve the real-time constrained optimal control decisions over a receding horizon. However, from the practice, it emerges that the coordinates of the virtual leader may fail very often to reach the end effector of the FFSM because of communication failure problems that are caused by many practical reasons. Therefore, a polynomial fitting algorithm is implemented in the NMPC controller based on Cramer's rule to predict the reference trajectory, which enhances the stability and robustness of the system and makes the manipulator capable to overcome efficiently the communication failure problems. The main novelty of this work is to cope with the above circumstances simultaneously in practice based on the NMPC approach, which is also found suitable to fulfill the physical limits of the system in real-time applications. At the end, the performance of the proposed approach is validated with a Matlab example, and the simulations results show the superiority and advantage of this work compared to the previous works in terms of efficiency and robustness.*

Keywords: *Communication Failure, Free-Floating Satellite Manipulator, Obstacle Avoidance, Nonlinear Model Predictive Control, Trajectory Tracking.*

1. Introduction

This paper focuses on the control of a Free-Floating Satellite Manipulator (FFSM) which consists mainly of a set of robotic manipulators that are tied to a satellite. The FFSM plays an important role to carry out different space missions [1–5]. In the literature, there is a huge volume of research work about the kinematics and dynamics control of the FFSM [6–10]. For example, trajectory tracking and obstacle avoidance are two fundamental tasks for the control of the FFSM in space applications. In one hand, the design of an efficient controller is extremely challenging because of nonlinearity and complexity of the FFSM. Thus, trajectory tracking approaches are proposed such that the FFSM is capable to realize path following efficiently. In [11] an optimization of the standard proportional integral derivative (PID) controller based on particle swarm optimization (PSO) algorithm is proposed, and an estimation algorithm is applied to deal with communication

failure problem, whereas the performance of the proposed PID-PSO controller is shown in comparison to the conventional PID controller and the PID optimized by genetic algorithm (PID-GA) controller. In [12], a nonsingular terminal sliding mode control strategy is developed with predefined-time stability for trajectory planning and control of a dual-arm free-floating space robot. In [13], a fuzzy sliding mode controller is used for trajectory tracking of the space robot to deal with external disturbance and parametric variation. On the other hand, space debris are considered as unwanted objects when the space robots are executing tasks. Therefore, the design of efficient methods to avoid obstacles in real-time applications is still a difficult research topic [14–17]. Traditionally, obstacle avoidance is treated as a high level planning task. For instance, in [18], a new path planning method is proposed based on an active set algorithm for a robotic arm mounted on the free-floating spacecraft, and its results are compared with the bidirectional Rapidly-exploring Random Trees (RRT) algorithm. In [19], an optimal path generator is proposed with a genetic algorithm and needs only the Cartesian position of the point to grasp as an input, without prior knowledge of a desired path. In [20], a model-free hierarchical decoupling optimization algorithm is developed to realize 6D-pose multi-target trajectory planning for the free-floating space robot.

Based on this background, it emerges that trajectory tracking of the space robot with obstacle avoidance and communication failure (CF) as a particular case, have been studied separately in the previous works, but in fact these problems may happen at the same time in practical applications. Therefore, the aim of this paper is to propose a novel control method that makes the FFSM capable to follow a reference path that is provided by a virtual leader robot while avoiding dynamic obstacles in real-time, and overcome the communication failure problems. The main idea behind the present work is the use of a nonlinear model predictive control (NMPC) approach. Although, the origins of this technique are the chemical plants and oil refineries, however the application of the MPC method has increased in the last decades to other fields like the space domain. For example in [21], a NMPC approach is proposed to trajectory tacking and obstacle avoidance of a free-floating space robot. In [22], a mixed integer predictive controller is developed for trajectory tracking and real-time obstacle avoidance of the FFSM. In [23], a NMPC is proposed for a rotation floating space robot and its efficacy is compared with Transpose Jacobian Cartesian (TJC) controller that is based on Generalized Jacobian Matrix (GJM).

According to the works [11] and [21], the main contribution of this paper is to propose for the first time a novel control approach for trajectory tracking of FFSM with real-time obstacle avoidance under the CF problem. At first, the anti-collision constraints are derived based on the velocity damper method, then they are integrated as inequality conditions within a quadratic programming (QP) process to get an optimal solution about the receding horizon. However, it emerges from the practice that CF might occur very often between the end effector and the virtual leader because of noise, external disturbances and errors in the sensors. To overcome this problem, a polynomial fitting algorithm is adopted in this paper based on Cramer's rule to predict the reference path of the virtual leader. To the best of the knowledge of the author, this work is the first that discusses the above circumstances in a unique a work for the control of the FFSM.

The remainder of this paper is structured as follows. Section 2. presents the dynamic model of the FFSM. Section 3. discusses the anti-collision constraints. Section 4. discusses in detail the proposed approach for the control of the FFSM. Section 5. demonstrates the simulation results to validate the proposed approach. Section 6. gives the main concluding remarks and the future works.

2. Modelling of the FFSM

A Free-Floating Satellite Manipulator (FFSM) is a mechanical system that is composed of the satellite as the base that is floating in space and a set of manipulators that are attached to the satellite. Assume the environment depicted in Figure 1, which consists of a FFSM with two

rigid links that is supposed to follow a reference path provided by a virtual leader robot on the space while avoiding moving obstacles in real-time. While taking into consideration the problem of communication failure between the virtual leader and the end effector. Table 1 contains the list of symbols that are used in this section.

According to the Lagrangian method (see Appendix B for more details), the FFSM model is given as follows.

$$\begin{bmatrix} H_b & H_{bm} \\ H_{bm}^T & H_m \end{bmatrix} \begin{bmatrix} \ddot{x}_b \\ \ddot{\theta} \end{bmatrix} + \begin{bmatrix} \dot{H}_b & \dot{H}_{bm} \\ \dot{H}_{bm}^T & \dot{H}_m \end{bmatrix} \begin{bmatrix} \dot{x}_b \\ \dot{\theta} \end{bmatrix} + \begin{bmatrix} c_b \\ c_m \end{bmatrix} = \begin{bmatrix} 0 \\ \tau \end{bmatrix} \tag{1}$$

where $\ddot{x}_b = (\ddot{r}_b, \dot{\omega}_b) \in \mathbb{R}^6$ denotes the vector of linear and angular accelerations of the base, and $\ddot{\theta} \in \mathbb{R}^n$ is the manipulator joint accelerations. The total momentum ($L_0 \in \mathbb{R}^6$) of the mass center of the system is deduced by the angular momentum conservation law as follows.

$$L_0 = H_b \dot{x}_b + H_{bm} \dot{\theta} \tag{2}$$

Suppose the initial momentum is zero ($L_0 = 0$), the dynamic formulation of the FFSM derived from equation 2 is given as follows.

$$\tau = H(\theta)\ddot{\theta} + c(\theta, \dot{\theta}) \tag{3}$$

where $H(\theta) = H_m - H_{hm}^T H_h^{-1} H_{bm} \in \mathbb{R}^{n \times n}$ is the generalized inertia matrix $c(\theta, \dot{\theta}) = c_m - H_{hm}^T H_b^{-1} c_b \in \mathbb{R}^{n \times 1}$ is the vector of the nonlinear force and the control torque of the FFSM.

3. Anti-collision constraints

Suppose $\mathcal{O}$ be a closed subset of R^3 and $X(\mathcal{O})$ is the inner part of $\mathcal{O}$. The object $\mathcal{O}$ is said to be strictly convex with the condition that any two points $(\forall a, b \in \mathcal{O})$ satisfy the following convex combination $a + (1-\sigma)b \in X(\mathcal{O})$ where $0 < \sigma < 1$.

Figure 2 displays the interconnection across two strictly convex objects $\mathcal{O}_1$ and $\mathcal{O}_2$ where P_1 and $P_1^{'}$ indiacte the nearest two points from $\mathcal{O}_1$ to $\mathcal{O}_2$. The distance $d = \left\| P_1 P_1^{'} \right\|$ is continuously

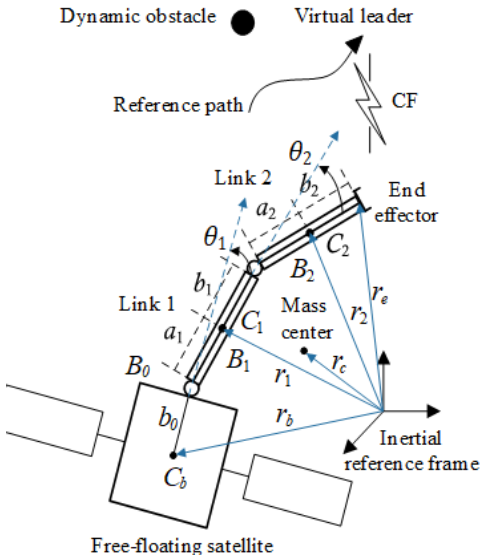

Fig. 1: FFSM scheme with moving obstacles.

Tab. 1: List of symbols.

Symbol	Representation
C_i	Link i mass center
J_i	Joint i
a_i	Position vector from J_i to C_i
b_i	Position vector from C_i to $J_(i+1)$
r_i	Link i position vector
r_b	Base position vector
r_e	End effector position vector
ω_b	Base angular velocity
ω_e	End effector angular velocity
m_i	Link i mass
I_i	Link i inertia matrix
H_b	Base inertia matrix
H_m	Manipulator inertia matrix
H_{bm}	Matrix of coupling inertia between base and manipulator
c_b	Vector of nonlinear coriolis
c_m	Vector of nonlinear centrifugal forces
τ	Torque control input

differentiable because both objects are strictly convex, and its derivative can be expressed as an inner product equation as follows

$$\dot{d} = < \dot{r}_{p_1} - \dot{r}_{p_1,}, n_1 > \tag{4}$$

where r_{pi} and $r_{pi'}$ denote the position and velocity vectors of point p_i. $n_1 = (r_{p_1} - r_{p_2})/d$ is a unit vector. Let $q = [x_b, \theta]^T$ and $\dot{q}$ be the FFSM configuration and generalized velocity, respec-

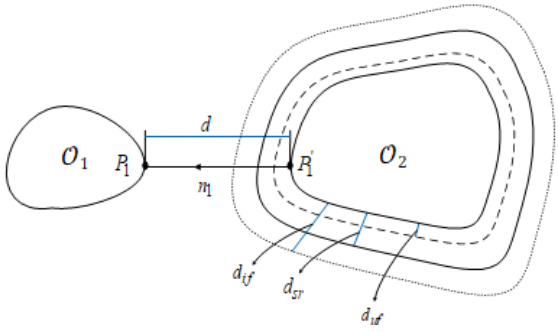

Fig. 2: The relationship between two objects

tively. Then the task-space velocity of P_i can be indicated by $\dot{r}_{p_i} = J_{p_i}\dot{q}$, where $J_{p_i} \in \mathbb{R}^{3\times(n+6)}$ is a Jacobian matrix of $\mathcal{O}_1$ at P_i. According to the velocity damper method, if d approaches into the influence distance (d_{if}), the following constraint is derived

$$\dot{d} \geq -\xi \frac{d - d_{uf}}{d_{if} - d_{uf}} \tag{5}$$

where $\xi\,(\xi > 0)$ is the parameter that is used for regulating the convergence speed, while $d_{uf}(d_{uf} < d_{if})$ is the unsafe distance with positive quantity.

If the initial condition $d(0) \geq d_{uf}$ is satisfied, then the velocity damper constraint can be derived in the following inequality.

$$d(t) \geq d_{uf} + (d(0) - d_{uf})\, e^{\frac{-\xi}{d_{if}-d_{uf}}t} > d_{uf}, \forall t > 0 \tag{6}$$

Equation 6 guaranties that the smallest distance among the two objects will be never lower than d_{uf} based on the velocity damper strategy.

With the same manner, another quantity named security distance is defined by $d_{uf} < d_{sr} < d_{if}$ which means that the inequality constraint of equation 5 will become a rigorous constraint if $d < d_{sr}$. It is worth noting that $\dot{d}$ is constrained by inequality 5 every time P_1 approaches the influence area $(d \leq d_{if})$. Then by plugging equation 4 into inequality 5, a linear inequality constraint about the generalized velocity $\dot{q}$ can be described as follows.

$$< J_{P_1}^T n_1, \dot{q} > \geq \langle \dot{r}_{p_1\prime}, n_1 \rangle - \xi \frac{d - d_{uf}}{d_{if} - d_{uf}} \tag{7}$$

The inequality constraints of equation 7 would be associated into the optimization problem in the next section.

4. Proposed approach

The general NMPC technique is summarized as follows.

$$u = \arg_u \min \Gamma\,(k) \tag{8}$$

Subject to

$$\begin{cases} x(k|k) = x_k \\ u(k+j|k) = u(k+N_c|k), j \geq N_c, \quad j \in [0, N_p - 1] \\ x(k+j+1|k) = f_d(x(k+j|k), u(k+j|k)) \\ y(k+j|k) = h_d(x(k+j|k), u(k+j|k)) \\ y_{min} \leq y(k+j|k) \leq y_{max} \\ u_{min} \leq u(k+j|k) \leq u_{max} \\ g(x(k+j|k)) \leq 0 \end{cases} \tag{9}$$

where the variables N_p and N_c denote respectively the prediction and the control horizon. k is the sampling time. The cost function $\Gamma(k)$ is a scalar amount. The two functions: $f_d(x(k+j|k), u(k+j|k))$ and $h_d(x(k+j|k), u(k+j|k))$ are the prediction and the measurement models. The inequality $g(x(k+j|k)) \leq 0$ denotes the supplementary constraints, like the security, terminal, and so forth.

At each sampling point k, the optimization is solved to get a series of optimal inputs as $\{u^*(k|k), ..., u^*(k+N_c-1|k)\}$. While a constrained QP process is adopted to get the optimal input whereas several constraints are involved in the optimization.

4.1. Optimization index

The quadratic form of the cost function that is used for the NMPC controller is expressed as follows.

$$\begin{aligned} \Gamma(k) = &\sum_{i=1}^{N_p} \|\hat{y}(k+i|k) - r(k+i|k)\|^2_{Q(i)} \\ &+ \sum_{i=0}^{N_c-1} \|\Delta\hat{u}(k+i|k)\|^2_{T(i)} \end{aligned} \tag{10}$$

where $Q(i)$ and $T(i)$ denote the tracking error and control effort matrix, respectively.

It should be noted that the dynamic model of the FFSM that is given in equation 3 cannot be applied directly in the MPC method because it is highly non-linear. Therefore, it needs to be transformed into a state-space form by using a feedback linearization procedure as follows.

Let $x = [\theta, \dot{\theta}]^T$ be the system states, and without considering the unmeasured noise, let $u = \ddot{\theta}$ be the new input of the system, then a state-space form in discrete-time can be established by the zero-order hold with a sampling period h as follows.

$$\begin{cases} x(k+1) = A_d x(k) + B_d u(k) \\ y(k+1) = C_d x(k+1) \end{cases} \tag{11}$$

where A_d, B_d and C_d are discrete-time matrices of the system, input and output, respectively. While $x(k), u(k)$ and$y(k)$ are respectively the vectors of states, input and output at time k.

The output of the system in equation 11 can be rewritten in the following form.

$$Y(k) = \Phi x(k) + \Upsilon u(k-1) + \Theta \Delta U(k) \tag{12}$$

where the matrices Φ, Υ and Θ might be given as follow:

$$\Phi = \begin{bmatrix} C_d A_d \\ \vdots \\ C_d A_d^{N_c} \\ C_d A_d^{N_c+1} \\ \vdots \\ C_d A_d^{N_p} \end{bmatrix}, Y = \begin{bmatrix} C_d B_d \\ \vdots \\ \sum_{i=0}^{N_c-1} C_d A_d^i B_d \\ \sum_{i=0}^{N_c} C_d A_d^i B_d \\ \vdots \\ \sum_{i=0}^{N_p-1} C_d A_d^i B_d \end{bmatrix},$$

$$\Theta = \begin{bmatrix} C_d B_d & \dots & 0 \\ \vdots & \ddots & \vdots \\ \sum_{i=0}^{N_c-1} C_d A_d^i B_d & \dots & C_d B_d \\ \sum_{i=0}^{N_c} C_d A_d^i B_d & \dots & \sum_{i=0}^{1} C_d A_d^i B_d \\ \vdots & \ddots & \vdots \\ \sum_{i=0}^{N_p-1} C_d A_d^i B_d & \dots & \sum_{i=0}^{N_p-N_c} C_d A_d^i B_d \end{bmatrix}.$$

Let the following expressions $Y(k) = [\hat{y}(k+1|k), ..., \hat{y}(k+N_p|k)]^T$, $R(k) = [r(k+1|k), ..., r(k+N_p|k)]^T$, and $\Delta U(k) = [\Delta\hat{u}(k|k), \dots, \Delta\hat{u}(k+N_c-1|k)]^T$, then the cost function $\Gamma(k)$ of equation 10 can be rewritten as follows:

$$\Gamma(k) = \|Y(k) - R(k)\|_Q^2 + \|\Delta U(k)\|_T^2 \tag{13}$$

where $Q = diag([Q(1), ..., Q(N_p)])$ and $T = diag([T(1), ..., T(N_c-1)])$. Let introduce a new variable $\epsilon(k)$ as follows:

$$\varepsilon(k) = R(k) - \Phi x(k) - \Upsilon u(k-1) \tag{14}$$

Hence, the cost function $\Gamma(k)$ of equation 13 might be rewritten as stated below.

$$\Gamma(k) = \|\Theta \Delta U(k) - \varepsilon(k)\|_Q^2 + \|\Delta U(k)\|_T^2 \tag{15}$$

which can be rewritten as follows:

$$\Gamma(k) = \Gamma_{\text{const}} + \Delta U(k)^T \vartheta + \Delta U(k)^T M \Delta U(k) \tag{16}$$

where $\Gamma_{\text{const}} = \varepsilon(k)^T Q \varepsilon(k), \vartheta = -2\Theta^T Q \varepsilon(k)$ and $M = \Theta^{\mathrm{T}} Q \Theta + \mathrm{T}$.

4.2. Inequality constraints

The optimal control issue over the receding horizon can be given as stated below.

$$\begin{cases} \Delta U^*(k) = \underset{\Delta U}{min}\, \Delta U(k)^T M \Delta U(k) + \vartheta^T \Delta U(k) \\ \text{Subject to } G \Delta U(k) \le g \end{cases} \tag{17}$$

Equation 17 is a constrained QP problem, and several constraints should be transformed into inequality equations. then getting the amounts of G and g.

Due to the fact that the inertia matrix $\mathrm{H}(\theta)$ is positive, then the limits in the new control input are given as follows.

$$\begin{cases} u_{min} = \hat{H}^{-1}(\underline{\tau} - \hat{c}) \\ u_{max} = \hat{H}^{-1}(\overline{\tau} - \hat{c}) \end{cases} \tag{18}$$

where $\underline{\tau} = \tau_{min}$ and $\overline{\tau} = \tau_{max}$ are the related torque vectors that comply with input boundary $(\tau_{min} \le \tau(t) \le \tau_{max} \forall t)$.

It is worth noting that the new input vector $u(t)$ does not mean it is the real control torque $\tau(t)$.

Given the dynamic model of equation 3 and the limits of the new input vector $u(k)$ in equation 18, this can be translated into linear inequalities around $\Delta U(k)$ as follows:

$$\Omega_{N_c} u_{min} \le \Omega_{N_c} u(k-1) + \Psi \Delta U(k) \le \Omega_{N_c} u_{max} \tag{19}$$

where the matrices Ω_{N_c} and Ψ can be expressed as follows: $\Omega_{N_c} = \begin{bmatrix} E_n \\ \vdots \\ E_n \end{bmatrix} \in \mathbb{R}^{nN_c \times n}$, $\Psi = \begin{bmatrix} E_n & & \\ \vdots & \ddots & \\ E_n & \dots & E_n \end{bmatrix} \in \mathbb{R}^{nN_c \times nN_c}$. Where $E_n \in \mathbb{R}^{n \times n}$ is a n dimensional identity matrix.

Likewise, suppose $Y_p = \Phi x(k) + \Upsilon u(k-1)$ and $\Omega_{N_n} = [E_{2n}, ..., E_{2n}]^T \in \mathbb{R}^{2nN_p \times 2n}$, where the limits in the system output are given as $(y_{min} \leq y(t) \leq y_{max} \ \forall t)$, then this can be translated as well into linear inequalities around $\Delta U(k)$ as follows.

$$\Omega_{N_p} y_{\min} \leq Y_p + \Theta \Delta U(k) \leq \Omega_{N_p} y_{\max} \tag{20}$$

while the FFSM configuration at one point falls inside the obstacle influence region, a consistent anti-collision constraint is actuated in the same way of equation 6.

Supposing that at time k, N_k anti-collision constraints are started and given the velocity-damper constraint in equation 7, hence this can be translated also into a linear inequality around $\Delta U(k)$ as follows.

$$D_{vp} + \Theta \Delta U(k) \geq D_{uf} \tag{21}$$

where $D_{vp} = \Theta_{vj} y_{vp}$ and $\Theta_v = \Theta_{vj} \Theta_{vb}$. Here, we choose $C_{vd} = [0_n, E_n]$ and define $y_{vp} = C_{vd} A_d x(k) + C_{vd} B_d u(k)$ and $\Theta_{vb} = [C_{vd} B_d, 0_n, ..., 0_n] \in \mathbb{R}^{n \times nN_c}$, in in the matter of equation 7, Θ_{vj} and D_{uf} can be formed as follows

$$\Theta_{vj} = \begin{bmatrix} n_1^T J_{P_1} \\ \vdots \\ n_i^T J_{P_i} \\ \vdots \\ n_{N_k}^T J_{P_{N_k}} \end{bmatrix}, D_{uf} = \begin{bmatrix} \langle \dot{r}_{p_2}, n_1 \rangle - \xi \frac{d_2 - d_{uf}}{d_{if} - d_{uf}} \\ \vdots \\ \langle \dot{r}_{p_i}, n_i \rangle - \xi \frac{d_i - d_{uf}}{d_{if} - d_{uf}} \\ \vdots \\ \langle \dot{r}_{p_{N_k}}, n_{N_k} \rangle - \xi \frac{d_{N_k} - d_{uf}}{d_{if} - d_{uf}} \end{bmatrix}.$$

while a range of constraints are modelled into inequality equations in the same way of equations 19,20 and 21, the values of G and g can be established as follows

$$G = \begin{bmatrix} \Psi \\ -\Psi \\ \Theta \\ -\Theta \\ -\Theta_v \end{bmatrix}, g = \begin{bmatrix} \Omega_{N_c} u_{\max} - \Omega_{N_c} u(k-1) \\ -\Omega_{N_c} u_{\min} + \Omega_{N_c} u(k-1) \\ \Omega_{N_p} y_{\max} - Y_p \\ -\Omega_{N_p} y_{\min} + Y_p \\ D_{vp} - D_{uf} \end{bmatrix}.$$

After getting the quantities of G and g, and by using the inequality of constraints of equation 17, the QP process is adopted to search the optimal control input in a receding horizon.

4.3. Communication failure

From the practice, it emerges that communication failure (CF) might occur very often between the end effector of the FFSM and the virtual leader robot because of many practical reasons such as noise, external disturbances that affect the stability of the system and errors in the sensors. Hence, these problems are taken into consideration in this paper. The CF event means that the coordinates of the reference trajectory (r) provided by the virtual leader fail to reach the end effector. Here, to overcome this problem then the value of the reference path (r) is replaced by an estimated function that is denoted by $\hat{r}$ which can be solved with a polynomial fitting algorithm along a directed axis of motion of the FFSM robot. Hence, the objective function $\Gamma(k)$ can be rewritten in as follows.

$$\begin{aligned} \Gamma(k) = (1-\lambda) \Bigg(& \sum_{i=1}^{Np} \|\hat{y}(k+i|k) - \\ & r(k+i|k)\|^2_{Q(i)} + \sum_{i=0}^{N_c-1} \|\Delta \hat{u}(k+i|k)\|^2_{T(i)} \Bigg) \\ & + \lambda \Big(\sum_{i=1}^{N_p} \|\hat{y}(k+i|k) - \hat{r}(k+i|k)\|^2_{Q(i)} \\ & + \sum_{i=0}^{N_c-1} \|\Delta \hat{u}(k+i|k)\|^2_{T(i)} \Big) \end{aligned} \tag{22}$$

where the variable λ has the following values, $\lambda = 0$ if there is no communication failure, and $\lambda = 1$ if there is a communication failure event. The estimated trajectory $\hat{r}$ can be approximated in the following form.

$$\hat{r} = a_K t^K + \cdots + a_1 t + a_0 + \epsilon \tag{23}$$

where a_K is the polynomial coefficient, $K$is the polynomial's degree, ϵ is the residual error.

The maximum order (K) of the polynomial is imposed by the number of data points used to generate the polynomial. The maximum order

of the polynomial for a set of N data points, is $K = N - 1$. In equation 23, the coefficients $(a_K, \ldots, a_1, a_0)$ are determined by solving the following equation.

$$\begin{bmatrix} N & \sum_{i=1}^{N} t_i & \cdots & \sum_{i=1}^{N} t_i^K \\ \sum_{i=1}^{N} t_i & \sum_{i=1}^{N} t_i^2 & \cdots & \sum_{i=1}^{N} t_i^{K+1} \\ \vdots & \vdots & \vdots & \vdots \\ \sum_{i=1}^{N} t_i^K & \sum_{i=1}^{N} t_i^{K+1} & \cdots & \sum_{i=1}^{N} t_i^{2K} \end{bmatrix} \begin{bmatrix} a_0 \\ a_1 \\ \vdots \\ a_K \end{bmatrix} = \begin{bmatrix} \sum_{i=1}^{N} t_i \\ \sum_{i=1}^{N} r_i t_i \\ \vdots \\ \sum_{i=1}^{N} r_i^K t_i \end{bmatrix} \tag{24}$$

Equation 24 is derived by the polynomial residual function and happens to be presented in the standard form $Ma = b$, which can be solved as follows.

$$a_k = \frac{\det(M_i)}{\det(M)} \tag{25}$$

where the matrix M_i is obtained from M by replacing its i^th column with the column vector b.

It should be noted that the estimation of the reference path is carried out along both axis of motion and the accuracy of tracking can be measured by the tracking error that is given as follows.

$$e(t) = \sqrt{(x_r - x)^2 + (y_r - y)^2} \tag{26}$$

where x_r and y_r represent the reference path coordinates along X-axis and Y-axis, respectively. While$x$ and y denote the actual coordinates of the FFSM.

The block diagram depicted in Figure 3 illustrates the proposed control system for the FFSM with NMPC controller and polynomial fitting algorithm to overcome CF problems. Depending on the value of λ, the estimation of the reference path ($i.e.$ $\hat{r}$) is used in case of CF.

5. Simulation results

This section demonstrates a simulation example that is validating the proposed control approach for trajectory tracking of FFSM with real-time obstacle avoidance and CF problems.

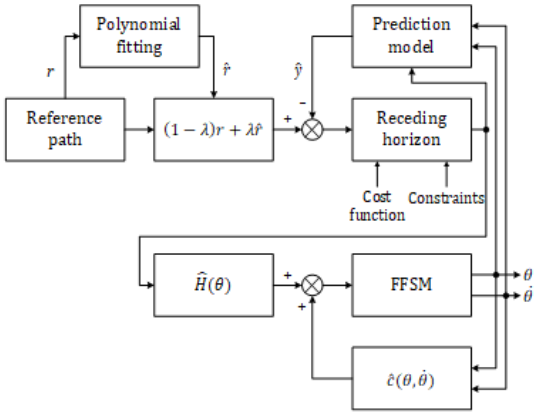

Fig. 3: Block diagram of the proposed approach.

Assume the FFSM shown in Figure 1 which consists of two rigid links, and the values of the inertia and mass for each link are indicated in Table 2. In this example, the FFSM is supposed to track a circle trajectory of the following coordinates: $x_r(t) = cos(t)$ and $y_r(t) = sin(t)$.

One sphere obstacle is placed in the workspace of the FFSM and it is supposed to move when the FFSM is performing path tracking and the robustness of the proposed approach is tested with two CF events.

Tab. 2: List of symbols.

Link	$a_i(m)$	$b_i(m)$	$m_i(kg)$	$I_i(kg.m^2)$
0	-	0.5	40	6.667
1	0.5	0.5	4	0.333
2	0.5	0.5	3	0.25

Figure 4 and Figure 5 show the time evolution of the tracking along X-axis and Y-axis, respectively. Where OA stands for obstacle avoidance. One can see in these figures that the end effector of the FFSM is executing tracking efficiently along both axes while it is avoiding the dynamic obstacle at two instants T_1 and T_2.

Now, the influences of the two CF events on the stability of the system can be seen clearly in Figure 6, which displays the time evolution of the tracking error as measured by equation 26. One can see in this figure that the polynomial fitting algorithm makes the FFSM capable of returning for tracking during CF events

1 and 2. In Figure 7, the result of trajectory tracking on the X-Y plane is depicted, in which the FFSM provided good tracking while avoiding the dynamic obstacle at times T_1 and T_2, and it is also verified that there is no influence of the CF events on the stability and robustness of the system.

Finally, it is concluded from these results that the proposed NMPC approach is more advantageous than the previous works in terms of stability and robustness of the manipulator. Moreover, it corresponds to human perception in dealing with such situations, and it can satisfy the physical limits of the system in practice.

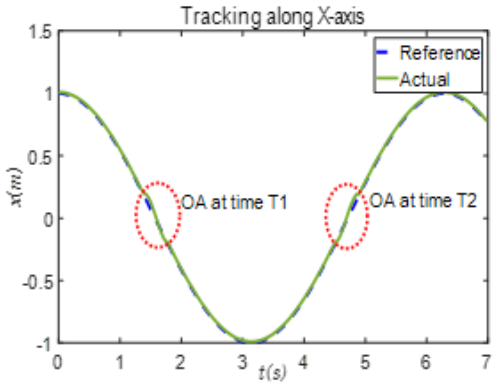

Fig. 4: Time evolution of FFSM tracking along X-axis.

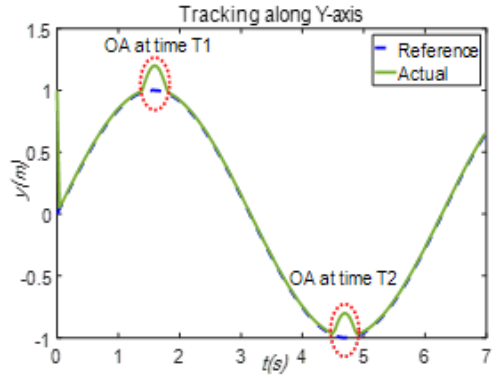

Fig. 5: Time evolution of FFSM tracking along Y-axis.

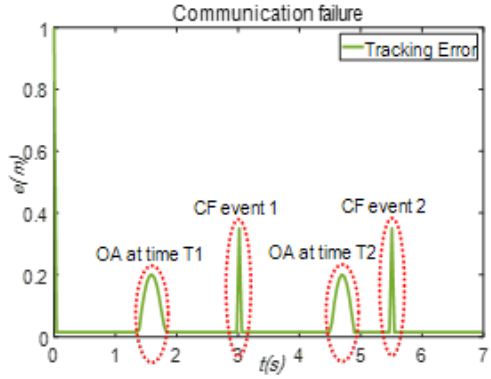

Fig. 6: Time evolution of the tracking error.

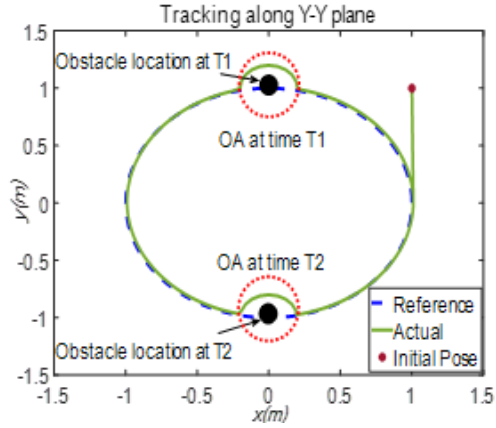

Fig. 7: Trajectory of the FFSM on the X-Y plane.

6. Conclusions

This paper proposes for the first time a unique approach for trajectory tracking of FFSM with real-time obstacle avoidance under the problem of CF between the end effector and the virtual leader. A robust optimization approach is proposed based on a nonlinear model predictive controller (NMPC). The anti-collision constraints are derived based on the velocity damper method, then they are integrated as inequality conditions in the NMPC within a quadratic programming (QP) process to get an optimal solution about the receding horizon. Moreover, a polynomial fitting algorithm is adopted based on Cramer's rule to predict the reference path in case of CF, which enhances the stability and robustness of the system, and it is very important for real-time applications.

The simulation results showed the efficiency of the proposed approach to make the FFSM capable to follow the reference path of the virtual leader while avoiding dynamic obstacles in real-time and the CF events are neglected based on the polynomial fitting algorithm. Hence, it is shown that this work has more advantages than the previous works for real-time applications.

Future works can consider the time delays and uncertainties in the FFSM model, also the detection of non-convex objects and the investigation of adaptive NMPC. Another future research is the application of the proposed approach to the formation control of multiple space robots.

Appendix A

The list of acronyms that are used in the paper are summarized in Table 3

Tab. 3: List of symbols.

Abb	Representation
FFSM	Free-Floating Satellite Manipulator
NMPC	Nonlinear Model Predictive Controller
QP	Quadratic Programing
PID	Proportional Integral Derivative
PSO	Particle Swarm Optimization
GA	Genetic Algorithms
RRT	Rapidly-exploring Random Trees
TJC	Transpose Jacobian Cartesian
GJM	Generalized Jacobian Matrix
CF	Communication Failure
OA	Obstacle Avoidance

Appendix B

The principle idea behind Lagrangian mechanics is the use of energies instead forces in order to derive the dynamic model of the system. In this paper, since the potential energy of the FFSM shown in Figure 1 is zero by assuming that the manipulator is rigid and operates in no gravity environment, then the Lagrangian (L) of the FFSM equals to the kinetic energy (K) and it is given as follows

$$L = K = \frac{1}{2}\left(\sum_{i=0}^{n}(\omega_i^{\mathrm{T}} I_i \omega_i + m_i r_i^T r_i)\right) \tag{27}$$

After simplification and rearrangement of terms, equation 27 can be rewritten as follows.

$$L = \begin{bmatrix}\dot{x_b}^T \dot{\theta}^T\end{bmatrix}\begin{bmatrix} H_b & H_{bm} \\ H_{bm} & H_m \end{bmatrix}\begin{bmatrix}\dot{x}_b \\ \dot{\theta}\end{bmatrix} \tag{28}$$

with H_b is the base inertia matrix, H_m is the manipulator inertia matrix, H_{bm} is the dynamic-coupling inertia matrix.

The Lagrangian equations of motion are given as follows:

$$\frac{d}{dt}\left(\frac{dL}{d\dot{x}_b}\right) - \frac{dL}{dx_b} = 0 \tag{29}$$

$$\frac{d}{dt}\left(\frac{dL}{d\dot{\theta}}\right) - \frac{dL}{d\theta} = 0 \tag{30}$$

By substituting the Lagrangian function expressed in Equation 28 into Equations 29 and 30, by computing the derivatives, and by properly rearranging the terms, the matricial equations of motion for the FFSM result as follows.

$$\begin{bmatrix} H_b & H_{bm} \\ H_{bm}^T & H_m \end{bmatrix}\begin{bmatrix}\ddot{x}_b \\ \ddot{\theta}\end{bmatrix} + \begin{bmatrix} \dot{H}_b & \dot{H}_{bm} \\ \dot{H}_{bm}^T & \dot{H}_m \end{bmatrix}\begin{bmatrix}\dot{x}_b \\ \dot{\theta}\end{bmatrix} + \begin{bmatrix} c_b \\ c_m \end{bmatrix} = \begin{bmatrix} 0 \\ \tau \end{bmatrix} \tag{31}$$

with the matrices c_b and c_m are defined as follows.

$$c_b = -\frac{\partial L}{\partial x_b} = -\frac{1}{2}\frac{\partial}{\partial x_b}\left(\dot{x}_b^T H_b \dot{x}_b + \dot{\theta}^T H_m \dot{\theta} + \dot{x}_b^T H_{bm}\dot{\theta} + \dot{\theta}^T H_{bm}^T \dot{x}_b\right) \tag{32}$$

$$c_m = -\frac{\partial L}{\partial \theta} = -\frac{1}{2}\frac{\partial}{\partial \theta}\left(\dot{x}_b^T H_b \dot{x}_b + \dot{\theta}^T H_m \dot{\theta} + \dot{x}_b^T H_{bm}\dot{\theta} + \dot{\theta}^T H_{bm}^T \dot{x}_b\right) \tag{33}$$

References

[1] G. Meng, L. Han, and C. Zhang. Research progress and technical challenges of space robot. *Acta Aeronaut. et Astronaut. Sinica*, 42(1):1–27, 2021.

[2] B. M. Moghaddam and R. Chhabra. On the guidance, navigation and control of in-orbit space robotic missions: A survey and prospective vision. *Acta Astronaut.*, 184:70–100, 2021.

[3] E. Papadopoulos, F. Aghili, O. Ma, and R. Lampariello. Robotic manipulation and capture in space: A survey. *Front. Robotics AI*, 8:686723, 2021.

[4] Y. Zhang, P. Li, J. Quan, L. Li, G. Zhang, and D. Zhou. Progress, challenges, and prospects of soft robotics for space applications. *Adv. Intell. Syst.*, 5(3):2200071, 2023.

[5] J. E. Lavín-Delgado, S. Chávez-Vázquez, J. F. Gómez-Aguilar, M. O. Alassafi, F. E. Alsaadi, and A. M. Ahmad. Intelligent neural integral sliding-mode controller for a space robotic manipulator mounted on a free-floating satellite. *Adv. Space Res.*, 49:3834–3844, 2019.

[6] E. Psomiadis and E. Papadopoulos. Model-based/model predictive control design for free-floating space manipulator systems. *30th Mediterr. Conf. on Control. Autom.*, pages 847–852, 2022.

[7] D. Shang, X. Li, M. Yin, J. Liu, and S. Zhou. Dynamic modeling and tracking control strategy for flexible telescopic space manipulator based on neural network compensation. *Adv. Space Res.*, 72(9):3645–3665, 2023.

[8] H. Yao, Y. Ren, and W. Wang. The control and simulation of space robot based on dynamically equivalent manipulator model. *Int. Conf. on Guid. Navig. Control.*, pages 1817–1828, 2020.

[9] T. Zhang, P. Shi, W. Li, and X. Yue. Ekf enhanced mpc for rapid attitude stabilization of space robots with bounded control torque in postcapture. *J. Frankl. Inst.*, 360(11):7105–7127, 2023.

[10] A. Alouache. Pid controller optimized based on pso for trajectory tracking of free-floating satellite robotic manipulator. *Braz. Technol. Symp.*, pages 83–92, 2023.

[11] Y. Liu, W. Yan, T. Zhang, C. Yu, and H. Tu. Trajectory tracking for a dual-arm free-floating space robot with a class of general nonsingular predefined-time terminal sliding mode. *IEEE Trans. on Syst. Man, Cybern. Syst.*, 52(5):3273–3286, 2021.

[12] E. W. Shibabw and G. Y. Tamiru. Fuzzy sliding mode controller based trajectory tracking control of free flying space robot manipulator system. *Int. Conf. on Adv. Sci. Technol.*, pages 137–158, 2022.

[13] A. Ledkov and V. Aslanov. Review of contact and contactless active space debris removal approaches. *Prog. Aerosp. Sci.*, 134:100858, 2022.

[14] V.A. Obukhov, V.A. Kirillov, V.G. Petukhov, A.I. Pokryshkin, G.A. Popov, V.V. Svotina, N.A. Testoyedov, and I.V. Usovik. Control of a service satellite during its mission on space debris removal from orbits with high inclination by implementation of an ion beam method. *Acta Astronaut.*, 19:390–400, 2022.

[15] V.V. Svotina and M.V. Cherkasova. Space debris removal–review of technologies and techniques. flexible or virtual connection between space debris and service spacecraft. *Acta Astronaut.*, 204:840–853, 2023.

[16] Y. Xu, X. Liu, R. He, Y. Zhu, Y. Zuo, and L. He. Active debris removal mission planning method based on machine learning. *Mathematics*, 11(6):1419, 2023.

[17] T. Rybus, M. Wojtunik, and F. L. Basmadji. Optimal collision-free path planning of a free-floating space robot using spline-based trajectories. *Acta Astronaut.*, 109:395–408, 2022.

[18] A. Seddaoui and C. M. Saaj. Collision-free optimal trajectory generation for a space robot using genetic algorithm. *Acta Astronaut.*, 179:311–321, 2021.

[19] S. Wang, Y. Cao, X. Zheng, and T. Zhang. Collision-free trajectory planning for a 6-dof free-floating space robot via hierarchical decoupling optimization. *IEEE Robotics Autom. Lett.*, 7(2):4953–4960, 2022.

[20] M. Wang, J. Luo, and U. Walter. A nonlinear model predictive controller with obstacle avoidance for a space robot. *Adv. Space Res.*, 57(8):1737–1746, 2016.

[21] L. Zong, J. Luo, M. Wang, and J. Yuan. Obstacle avoidance handling and mixed integer predictive control for space robots. *Adv. Space Res.*, 61(8):1997–2009, 2018.

[22] R. Srivastava, R. Sah, and K. Das. Nonlinear model predictive control of rotation floating space robots for autonomous active debris removal. *IFAC-PapersOnLine*, 55(22):147–152, 2022.

[23] F. Kanehiro, F. Lamiraux, O. Kanoun, E. Yoshida, and J. Laumond. A local collision avoidance method for non-strictly convex polyhedra. *Robotics Sci. Syst. IV*, pages 151–158, 2009.

About Authors

Ali ALOUAHE received his PHD degree in control systems engineering in June 2018 from the automation school of the Beijing Institute of Technology, PR China. He received the degree of magister of science in September 2014 from the Ecole Militaire Polytechnique of Bordj El Bahri, Algiers, Algeria. He obtained the engineer degree from the institute of electrical engineering and electronics at Boumerdes University, Algeria, in June 2012. Currently, he is a researcher at the Centre des Techniques Spatiales of the Algerian Space Agency in Arzew, Algeria. His research interests include robotics, image processing, computer vision, optimization, etc. He has many publications in international journals and conferences in the field of robotics and image processing.

